Eur. Phys. J. Plus (2017) **132**: 387
DOI 10.1140/epjp/i2017-11633-3

THE EUROPEAN PHYSICAL JOURNAL PLUS

Regular Article

Joule heating effect on a continuously moving thin needle in MHD Sakiadis flow with thermophoresis and Brownian moment

C. Sulochana[a], G.P. Ashwinkumar, and N. Sandeep

Department of Mathematics, Gulbarga University, Gulbarga - 585106, India

Received: 12 June 2017 / Revised: 3 July 2017
Published online: 13 September 2017 –

Abstract. In the current study, we investigated the impact of thermophoresis and Brownian moment on the boundary layer 2D forced convection flow of a magnetohydrodynamic nanofluid along a persistently moving horizontal needle with frictional heating effect. The various pertinent parameters are taken into account in the present analysis, namely, the thermophoresis and Brownian moment, uneven heat source/sink, Joule heating and frictional heating effects. To check the variation in the boundary layer behavior, we considered two distinct nanoparticles namely $Al_{50}Cu_{50}$ (alloy with 50% alumina and 50% copper) and Cu with water as base liquid. Numerical solutions are derived for the reduced system of governing PDEs by employing the shooting process. Computational results of the flow, energy and mass transport are interpreted with the support of tables and graphical illustrations. The obtained results indicate that the increase in the needle size significantly reduces the flow and thermal fields. In particular, the velocity field of the Cu-water nanofluid is highly affected when compared with the $Al_{50}Cu_{50}$-water nanofluid. Also, we showed that the thermophoresis and Brownian moment parameters are capable of enhancing the thermal conductivity to a great extent.

Nomenclature

U_0	Composite velocity
u_0, u_∞	Velocity of the needle and velocity of the main stream
T_0, T_∞	Temperature at the surface and ambient (K)
$\bar{c}$	Thickness of the needle
k_f	Thermal conductivity of the base fluid
k_s	Thermal conductivity of the solid particles
Pr	Prandtl number
M	Magnetic field parameter
Ec	Viscous dissipation
D_B	Brownian coefficient
D_T	Thermophoretic coefficient
Nb	Brownian motion parameter
A, B, K, E	Constants
Nt	Thermophoresis parameter
A^*	Space-dependent heat source/sink
B^*	Temperature-dependent heat source/sink
S_c	Schmidt number
C_f	Skin friction coefficient
Nu_x	Local Nusselt number
Sh_x	Local Sherwood number
Re_x	Reynolds number ($U_0\bar{x}/\nu_f$)

Greek letters

τ_w	Surface shear stress
θ	Dimensionless temperature
ξ	Dimensionless concentration
ρ_{nf}	Density of the nanofluid
μ_{nf}	Dynamic viscosity of the nanofluid
ϕ	Solid volume fraction
ρ_f	Density of the base fluid
ρ_s	Density of the nanoparticle
ν_f	Kinematic viscosity
$(\rho C_p)_{nf}$	Specific heat capacity of the nanofluid at constant pressure
$(\rho C_p)_f$	Heat capacity of the base fluid at constant pressure
$(\rho C_p)_s$	Heat capacity of the nanoparticle
ψ	Stream function
η	Similarity variable
γ	Velocity ratio parameter

[a] e-mail: maths.sulochana@gug.ac.in

1 Introduction

Conventional base fluids like water, kerosene, grease, oil, and mixtures of fluids possess very low thermal conductivity, as witnessed by the great number of industries dealing with such traditional base fluids. Nevertheless, they come across many problems due to their inefficiency in thermal conductivity. One of the powerful technique to overcome this deficiency is the amalgamation of nano-scaled elements in base liquids. This technique is commonly referred to as nanofluids technique. Nanofluids possess an enormous thermal conductivity in contrast with base liquids. During the past two decades, this new class of fluids has drawn the attention of a considerable number of researchers. Utilization of nanotechnology can be a life saver in diversified sectors of science and technology. Especially, in medical science, drug delivery for the treatment of cancer; in cooling processes, cooling of the nuclear reactor, industrial cooling, cooling of electronic equipments; in space vehicles, solar energy and much more. Nanotechnology was used by Murshed *et al.* [1] to enhance the heat transmission of water by the amalgamation of titania nano materials. Later on, Hatami *et al.* [2] discovered that the homotopy analysis method (CHAM) is more effective than the Runge-Kutta (R-K) method in solving the problem of a nanofluid flow past a slendering extending sheet. This study was continued by Sheikholeslami *et al.* [3] for the flow over a horizontal plate with dissipation effect. They revealed that the dissipation parameter significantly diminishes the energy transport. Malvandi *et al.* [4] implemented a mathematical model to incorporate the nanoparticle migration in the flow along a circular pipe. A comparative analysis has been carried out by Sulochana *et al.* [5] for the Casson nanofluid flow over an expanding surface and obtained dual solutions for Newtonian and non-Newtonian fluid by employing the R-K scheme. Further, Makinde *et al.* [6] determined the impact of variable gumminess on an electrically conducting nanofluid towards a radially extending surface.

Brownian motion emerges by virtue of the irregular motion of the nanoparticles in the amalgamation of solid-liquid materials and it is in proportion with the concentration gradient of the nanomaterial. Thermophoresis induces the motion of nanoparticles in a reversible manner with respect to the thermal gradient of the nanomaterial, which in turn causes the irregular dispersion of the volume fraction of nanomaterials. Thermophoresis and Brownian moment are key aspects of the migration of nanomaterials in nanofluids, as claimed by Buongirno [7]. The impact of thermophoresis and Brownian diffusion on the flow of a nanofluid caused by a stretching surface with varying thickness was presented by Babu and Sandeep [8]. They found dual solutions for water-based graphene and magnetic nanofluids. Sulochana *et al.* [9] proposed a Carreau mathematical model to elaborate the impact of suction and blowing on the stagnation-point flow of a nanofluid utilizing the Buongirno slip mechanism. Later on, some researchers [10,11] employed these slip mechanisms in their studies.

A thin needle is a slendering object with parabolic revolution and the flow caused by the thin needle is axisymmetric in nature, as the radius of the slendering needle is the same as that of the boundary layers established by the flow. The boundary layer flow due to a slendering needle with irregular thickness is a topic of the greatest practical importance. Since it has been utilized in many areas of science and engineering, viz. biological sciences: in cancer treatment, blood flow problems; industries: in metal spinning, in aerodynamics, in paper production, in small measuring equipment, etc. Initially, Lee [12] elaborated the axisymmetric flow of a viscous fluid caused by a slendering needle with paraboloid revolution about the axis. He concluded that the paraboloid turns into a line along the axis due to the decrease in the needle size. Later on, Wang [13] explored the impact of a free/forced convection flow on a slendering object (needle) with paraboloid revolution. They used the adiabatic process and the heat source at the edge. The free convection flow of a viscous fluid towards a slendering surface with irregular temperature was proposed by Grosan and Pop [14]. They obtained numerical solutions in the presence of copper and alumina nano-scaled elements. Further, few researchers [15–17] investigated the boundary layer behaviour of an incessantly moving slendering needle. They incorporated diversified nanomaterials with accompanying water as a base liquid.

Moreover, Prasad *et al.* [18] studied the impact of an external magnetic field on the flow past a stretchable surface with irregular thickness. In their analysis, they presumed a decrease in surface temperature and velocity. The authors [19,20] examined the mixed convection flow caused by a slendering surface of varying thickness by using the R-K scheme. They analyzed the flow under the impact of cross diffusion and slip mechanism. Further, the researchers [21,22] investigated the bio-convection nanofluid flow across a slendering sheet with ferrous nanoparticles and gyrotactic micro-organisms. The combined natural and forced convection flow over objects of dissimilar geometries, *i.e.* cylinder and vertical cone, in a nanofluid was reported by Nazar *et al.* [23] and Patrulescu *et al.* [24], respectively. Here the authors analyzed the problem by using CuO, Al_2O_3 and TiO_2 nanoparticles. Reddy *et al.* [25] proposed a model to address the MHD flow mechanism over objects of dissimilar geometries, namely cone, wedge and plate. They showed that the probe of thermal relaxation is to diminish the fluid temperatures. Very recently, few authors [26–29] examined the natural, forced and mixed convection flow over diversified geometrical objects such as vertical cone, vertical cylinder and wedge, embedded in porous media. Khan *et al.* [30] explained the heat transport nature of the flow of a ferrofluid induced by a flat plate at a constant temperature. The impact of an external magnetic field on convective heat transfer in ferrofluids was analysed by Sheikholeslami and Ganji [31]. Relevant research in this regard can be found in the literature [32,33].

To the authors' knowledge, only a few researchers made an attempt to use the aluminium and copper alloys in their analysis. Due to their substantial properties, such as an extremely high corrosion resistance, extraordinary electrical and thermal conductivities and ease of fabrication, they achieved remarkable applications in transportation,

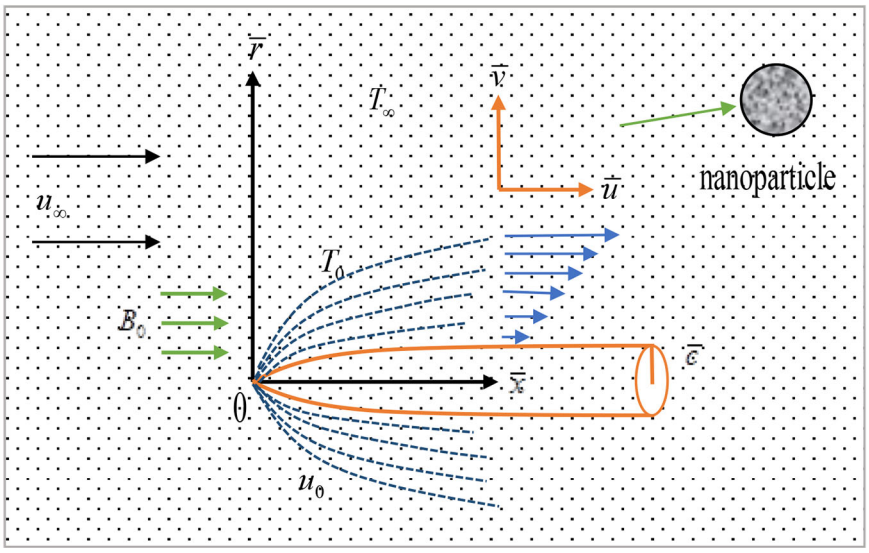

Fig. 1. Flow geometry.

especially in space and aircraft, in the production of electrical transmission lines. With the aim to fill the gap of Soid *et al.* [17], in this paper we discussed the boundary layer analysis of a magneto hydrodynamic flow along a persistently moving thin needle by considering the thermophoresis and Brownian moment effects. We incorporated the Joule heating, frictional heating, nanoparticle volume fraction, variable heat source/sink effects over momentum, energy and concentration distributions. To check the variation in the boundary layer behavior, we utilized distinct nanoparticles namely, $Al_{50}Cu_{50}$ alloy and Cu, which are suspended in water. The system of flow-governing PDEs is solved numerically by employing shooting technique.

2 Formulation of the problem

We assumed a time-independent, 2D dissipative magnetic-nanofluid flow over a persistently moving thin needle as displayed in fig. 1. Here $(\bar{x}, \bar{r})$ represent the axial and radial coordinates in cylindrical form, respectively, and $\bar{c}$ is the thickness of the needle. The size of the needle is thin, as its variable thickness is not greater than the boundary layer formed on it.

The governing equations of the flow in the above-mentioned circumstances in cylindrical coordinates are

$$(\bar{r}\bar{u})_{\bar{x}} + (\bar{r}\bar{v})_{\bar{r}} = 0, \tag{1}$$

$$\rho_{nf}\left\{\bar{u}(\bar{u}_x) + \bar{v}(\bar{u}_r)\right\} = \mu_{nf}(\bar{r}^{-1})\left\{\bar{r}(\bar{u}_r)\right\}_r - \sigma_{nf}B_0^2\bar{u}, \tag{2}$$

$$(\rho C_p)_{nf}\left\{\bar{u}(T_{\bar{x}}) + \bar{v}(T_{\bar{r}})\right\} = k_{nf}(\bar{r}^{-1})\left\{\bar{r}(T_{\bar{r}})\right\}_{\bar{r}} + \tau\left\{D_B C_{\bar{r}} T_{\bar{r}} + (D_T/T_\infty)(T_{\bar{r}})^2\right\} + q''' + \sigma_{nf}B_0^2\bar{u}^2 + \mu_f(\bar{u}_{\bar{r}})^2, \tag{3}$$

$$\left\{\bar{u}(C_{\bar{x}}) + \bar{v}(C_{\bar{r}})\right\} = (D_T/T_\infty)(\bar{r}^{-1})\left\{\bar{r}(T_{\bar{r}})\right\}_{\bar{r}} + D_B(\bar{r}^{-1})\left\{\bar{r}(C_{\bar{r}})\right\}_{\bar{r}}, \tag{4}$$

the appropriate boundary limitations are

$$\begin{aligned} &\bar{u} = u_0, \quad \bar{v} = 0, \quad T = T_0, \quad C = C_0 \quad \text{at } \bar{r} = R(\bar{x}), \\ &\bar{u} \to u_\infty, \quad T \to T_\infty, \quad C \to C_\infty \quad \text{as } \bar{r} \to \infty, \end{aligned} \tag{5}$$

where the velocity components in the x- and y-direction are $\bar{u}$ and $\bar{v}$, respectively, $R(x)$ represents the surface shape of the thin needle. The effective nanofluid properties are given as

$$\begin{aligned} &\rho_{nf} = (1-\phi)\rho_f + \phi\rho_s, \qquad \mu_{nf} = \mu_f(1-\phi)^{-2.5}, \qquad (\rho C_p)_{nf} + \phi(\rho C_p)_f = (\rho C_p)_f + \phi(\rho C_p)_s, \\ &k_{nf} = \left(\frac{k_s + 2k_f - 2\phi k_f + 2\phi k_s}{k_s + 2k_f + 2\phi k_f - 2\phi k_s}\right)k_f, \qquad \frac{\sigma_{nf}}{\sigma_f} = \left[1 + \frac{3(\sigma-1)\phi}{(\sigma+2) - (\sigma-1)\phi}\right], \quad \sigma = \frac{\sigma_s}{\sigma_f}. \end{aligned} \tag{6}$$

The uneven heat source/sink q''' can be expressed as

$$q''' = \frac{k_f u_0}{x\nu_f}[A^*(T_0 - T_\infty) + B^*(T - T_\infty)]. \tag{7}$$

The following similarity transformations are used to reduce eqs. (1)–(4) to the dimensionless form

$$\psi = \nu_f \bar{x} f(\eta), \qquad \theta = (T - T_\infty)/(T_0 - T_\infty), \qquad \xi = (C - C_\infty)/(C_0 - C_\infty), \qquad \eta = U_0 \bar{r}^2/\nu_f \bar{x},$$
$$\bar{u} = (1/\bar{r})\psi_r, \qquad \bar{v} = (-1/\bar{r})\psi_x, \qquad R(\bar{x}) = (\nu_f \bar{x}\bar{c}/U)^{1/2}. \tag{8}$$

Setting $\eta = \bar{c}$ in eq. (7) describes the size and shape of the thin needle $\bar{r} = R(\bar{x})$.

Equation (1) is automatically satisfied, further eqs. (2)–(4) are reduced to

$$(2Af'''\eta + 2Af'') + B(ff'' - M\sigma_{nf} f') = 0, \tag{9}$$
$$2K(\theta''\eta + \theta') + \Pr E f\theta' + (A^* f' + B^*\theta) + \Pr Ec(2\eta f''^2 + M\sigma_{nf} f'^2) + 2\eta\left\{Nb\theta'\xi' + Nt(\theta')^2\right\} = 0, \tag{10}$$
$$\xi''\eta + \xi' + (Nt/Nb)(\theta''\eta + \theta') + (S_c/2) f\xi' = 0, \tag{11}$$
$$A = (1-\phi)^{-5/2}, \qquad B = 1 - \phi + \phi(\rho_s/\rho_f), \qquad K = k_{nf}/k_f, \tag{12}$$

where $E = 1 - \phi + \phi\{(\rho C_p)_s/(\rho C_p)_f\}$.

The transformed boundary conditions are

$$f(\eta) = \frac{\gamma\bar{c}}{2}, \quad f'(\eta) = \frac{\gamma}{2}, \quad \theta(\eta) = 1, \quad \xi(\eta) = 1, \quad \text{at } \eta = \bar{c},$$
$$f'(\eta) \to (1-\gamma)/2, \quad \theta(\eta) \to \gamma/2, \quad \xi(\eta) \to \gamma/2 \quad \text{as } \eta \to \infty, \tag{13}$$

where the prime denotes derivative w.r.t. η, and M, Pr, Ec, Nt, Nb, γ, U_0 and S_c are dimensionless parameters expressed as

$$M = \sigma_f B_0^2/2U_0\rho_f, \qquad \Pr = \mu_f C_p/k_f, \qquad Ec = (2U_0^2)/C_p(T_0 - T_\infty), \qquad \gamma = u_0/U_0, \qquad S_c = \nu/D_B,$$
$$U_0 = u_0 + u_\infty, \qquad Nb = \tau D_B(C_0 - C_\infty)/\nu_f k_f, \qquad Nt = \tau D_T(T_0 - T_\infty)/T_\infty \nu_f k_f. \tag{14}$$

The physical quantities of practical interest are C_f, Nu_x and Sh_x which are as follows:

$$\frac{\mathrm{Re}_x^{0.5}}{4(\bar{c})^{0.5}A} C_f = f''(\bar{c}),$$
$$\frac{\mathrm{Re}_x^{-0.5}}{2(\bar{c})^{0.5}K} Nu_x = -\theta'(\bar{c}),$$
$$\frac{\mathrm{Re}_x^{-0.5}}{2(\bar{c})^{0.5}D_B} Sh_x = -\xi'(\bar{c}). \tag{15}$$

3 Discussion of the results

In this section we give, the impact of various physical parameters on the flow, mass and energy transfer distributions of two distinct nanofluids namely $Al_{50}Cu_{50}$-water and Cu-water. The transformed dimensionless flow-governing eqs. (9), (10) and (11) with relevant boundary restrictions (13) are numerically solved by employing the shooting process. The impact of the pertinent parameters such as ϕ, M, Nt, Nb, Ec, A^*, B^* and $\bar{c}$ on the flow, mass, and energy transport behavior of the fluid, with Nu_x, Sh_x and C_f is presented with the support of graphs and tabular values. Certain parametric values are kept constant, *i.e.* $\phi = 0.2$; $M = 1$; $A^* = 0.1$; $B^* = 0.1$; $\gamma = 1$; $\bar{c} = 0.1$; $Nt = 0.5$; $Nb = 0.5$; $S_c = 1$; $Ec = 0.1$ in the overall study, except for the changes in the parametric values which are mentioned in figs. 2–19 and tables 2 and 3.

Figures 2–4 and 5–7 show the velocity, thermal and concentration behavior for increasing values of M and ϕ. As observed, the rise in M and ϕ leads to a similar tendency with respect to velocity, thermal and concentration fields. These parameters make the velocity and concentration fields decrease, but augment the thermal fields. Physically, increasing values of M cause the onset of a resistive type of force, referred to as Lorentz force. The existence of this force may lead to the decrease of the momentum and concentration fields, whereas it enhances the thermal boundary layer thickness. Figures 5–7 reveal that increasing values of ϕ make the velocity and concentration distribution drop, but they regulate the thermal distribution. Generally, an increase in ϕ leads to strengthening the fluid viscosity. Consecutively, a highly viscous fluid possesses lesser velocity. Thus, we perceive a decrease in velocity and concentration fields and a rise in thermal fields. It is interesting to note that the $Al_{50}Cu_{50}$-water nanofluid possesses a significantly higher velocity compared with the Cu-water nanofluid.

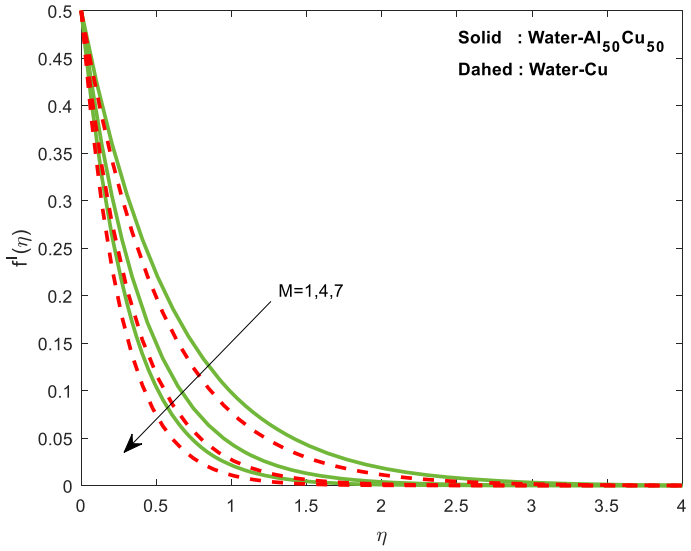

Fig. 2. Velocity behavior with variation in M.

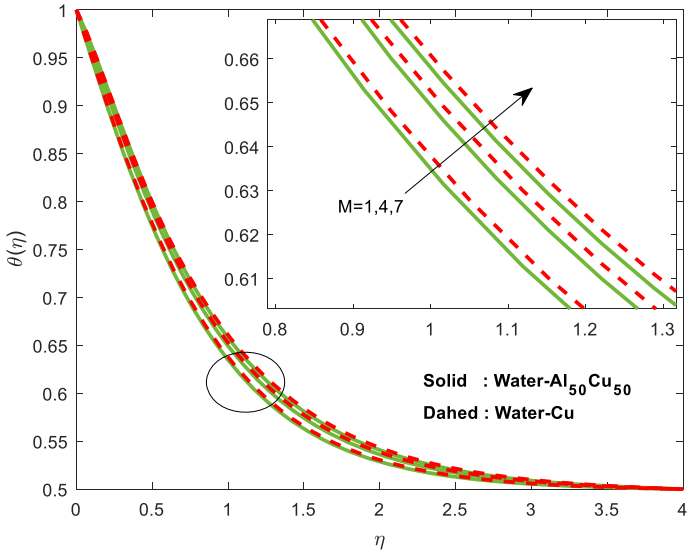

Fig. 3. Thermal behavior with variation in M.

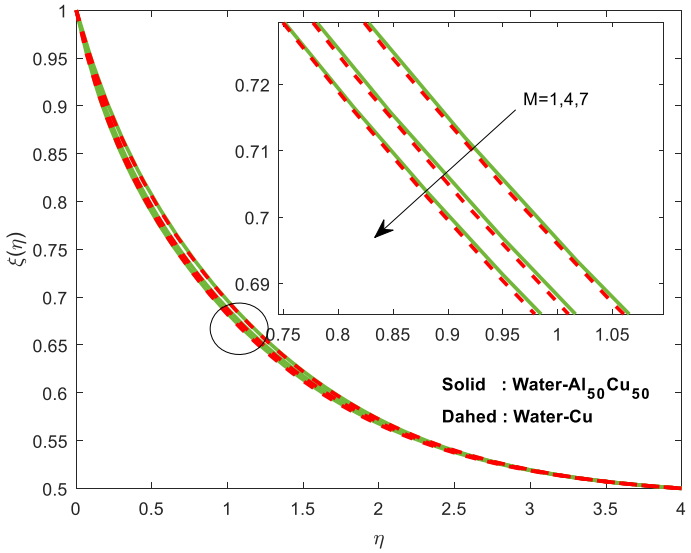

Fig. 4. Concentration behavior with variation in M.

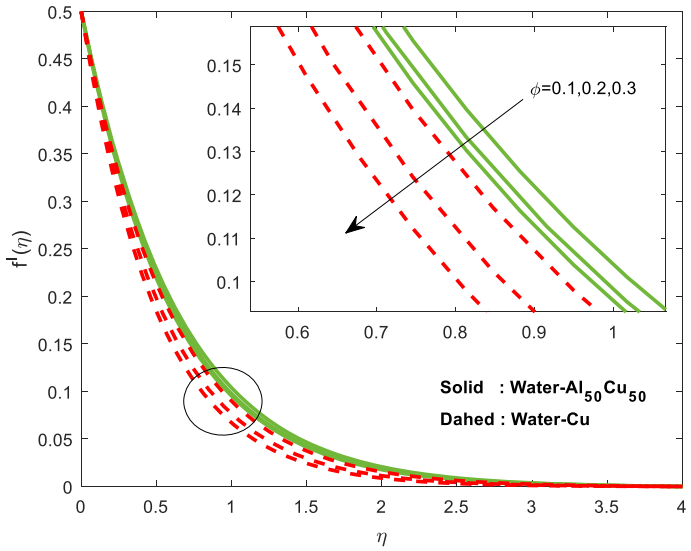

Fig. 5. Velocity behavior with variation in ϕ.

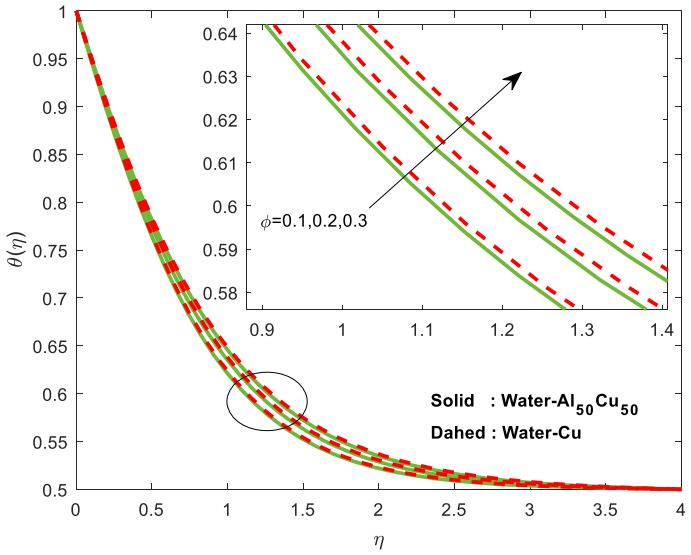

Fig. 6. Thermal behavior with variation in ϕ.

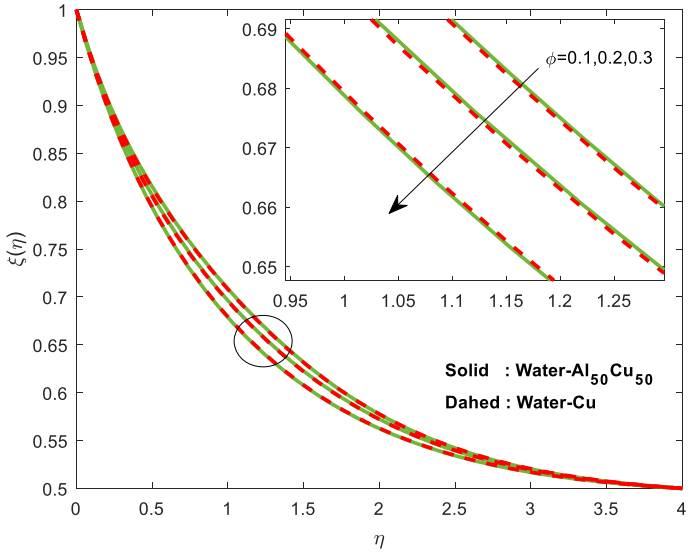

Fig. 7. Concentration behavior with variation in ϕ.

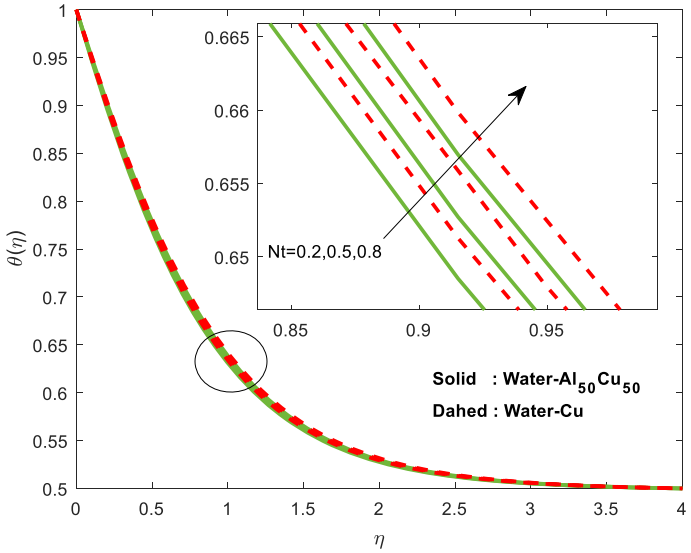

Fig. 8. Thermal behavior with variation in Nt.

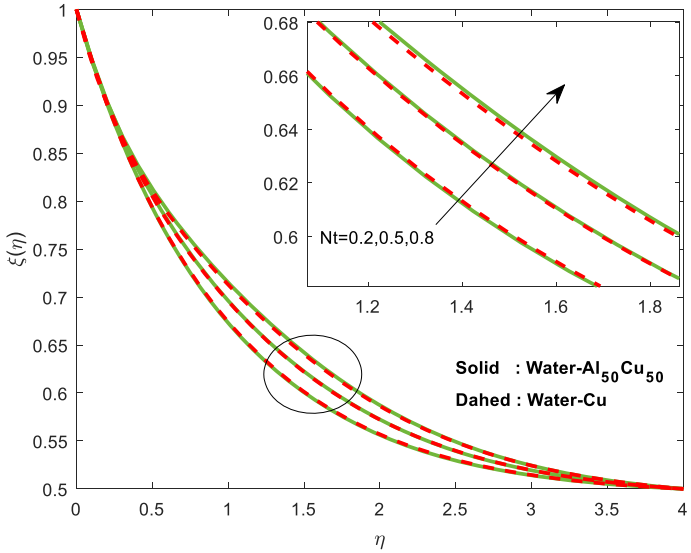

Fig. 9. Concentration behavior with variation in Nt.

The impact of an increasing value of Nt and Nb on the thermal and concentration distribution is investigated in figs. 8–11, respectively. It is found that the thermal field is an increasing function of Nt and Nb. But, a reverse behaviour can be seen for the concentration fields. Physically, the increase in Nt and Nb enhances the thermal conductivity of the fluid. Brownian motion has a reciprocal behaviour with respect to the concentration distributions. Hence, we obtain a reverse trend in the concentration fields. Figure 12 is devoted to monitoring the impact of increasing values of Ec on thermal fields. It can be seen that the rising value of Ec enhances the fluid velocity near the surface, as a result, it produces a large friction near the surface. Due to this, a decrease in the thermal filed of the fluid is observed.

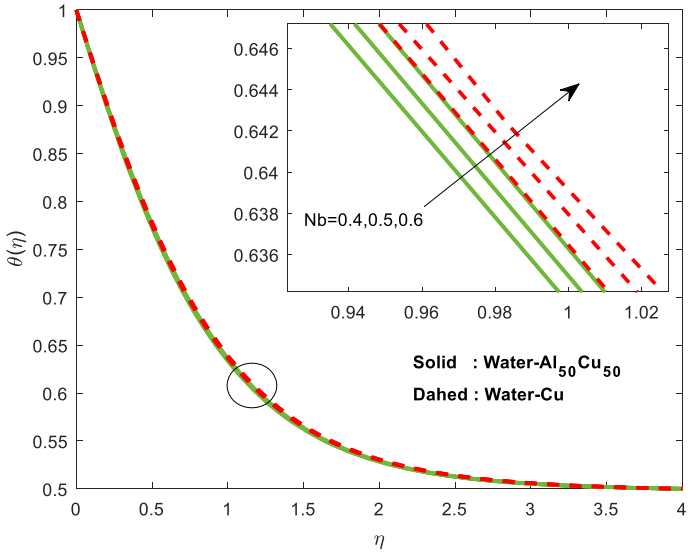

Fig. 10. Thermal behavior with variation in Nb.

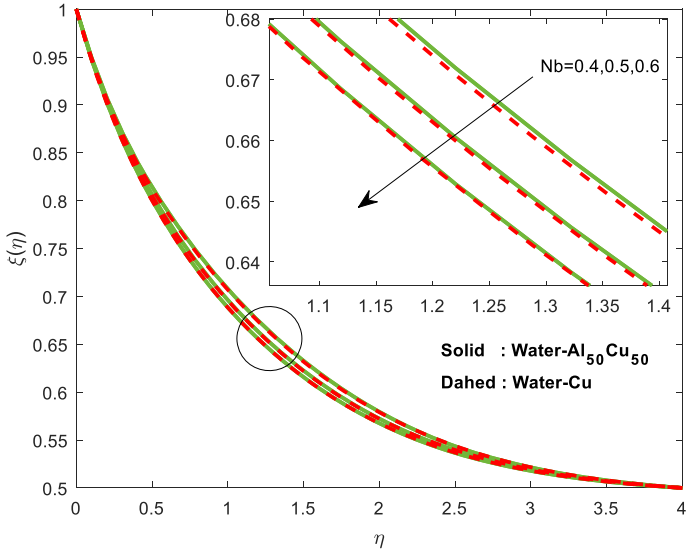

Fig. 11. Concentration behavior with variation in Nb.

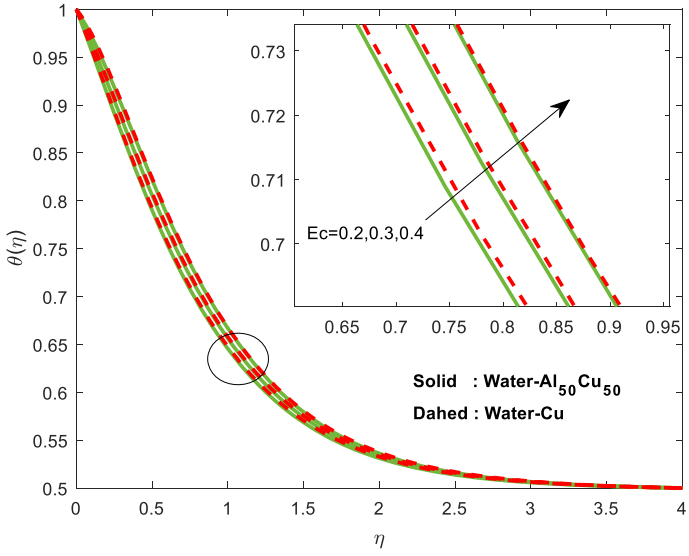

Fig. 12. Thermal behavior with variation in Ec.

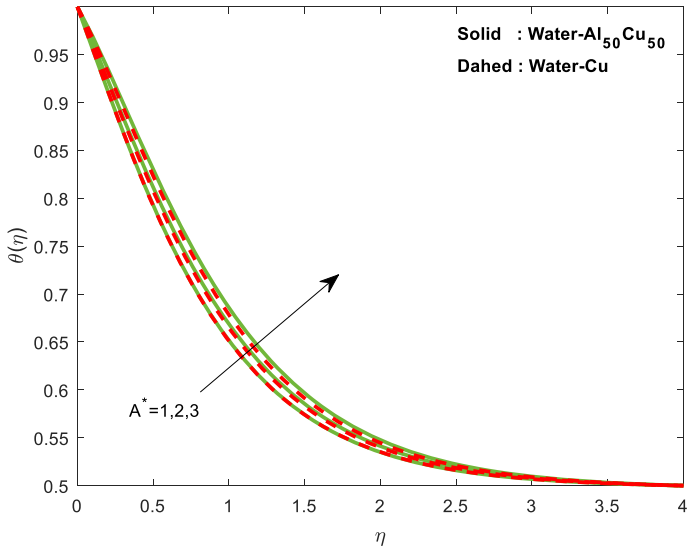

Fig. 13. Thermal behavior with variation in A^*.

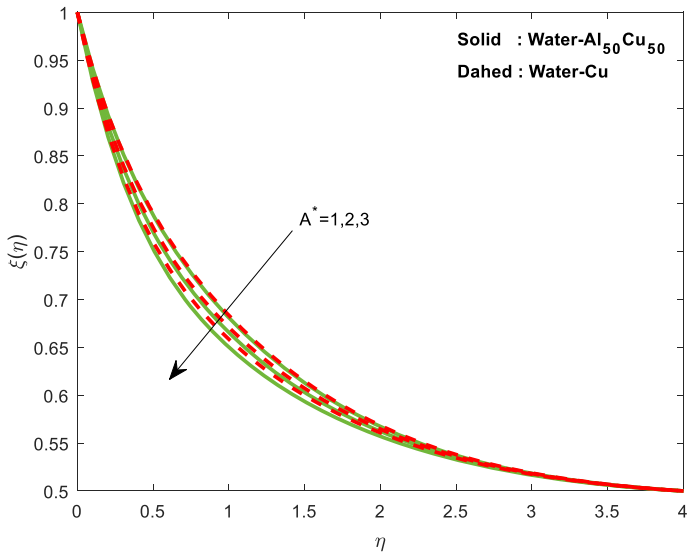

Fig. 14. Concentration behavior with variation in A^*.

The behaviour of the thermal and concentration fields for increasing values of A^* and B^* is shown in figs. 13–16, respectively. As seen, increasing values of A^* and B^* make the fluid temperature rise, but make the concentration fields decrease. Generally, positive values of A^* and B^* supply heat energy to the fluid and negative values of A^* and B^* subtract heat energy from it. Hence, we found an increase in fluid temperature and a drop of the concentration fields of the fluid. It is appearing to claim that, the thermal boundary thickness of the $Al_{50}Cu_{50}$-water nanofluid is slightly higher than that of the Cu-water nanofluid. But, a reverse behaviour is found in the concentration behavior. Figures 17–19 are plotted to study the nature of the velocity, thermal and concentration fields with increasing values of $\bar{c}$. It is apparent that increasing the needle size disturbs the free stream, which in turn causes to diminish the fluid velocity. As a result, we found a drop in the velocity and thermal fields and an enhancement in the concentration fields.

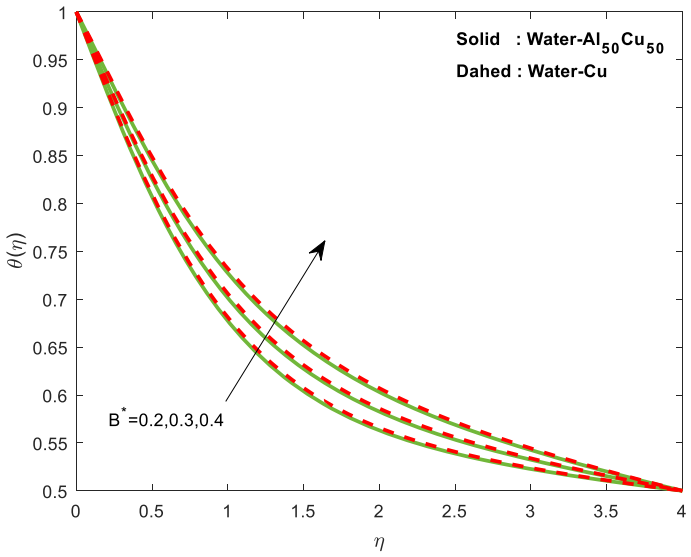

Fig. 15. Thermal behavior with variation in B^*.

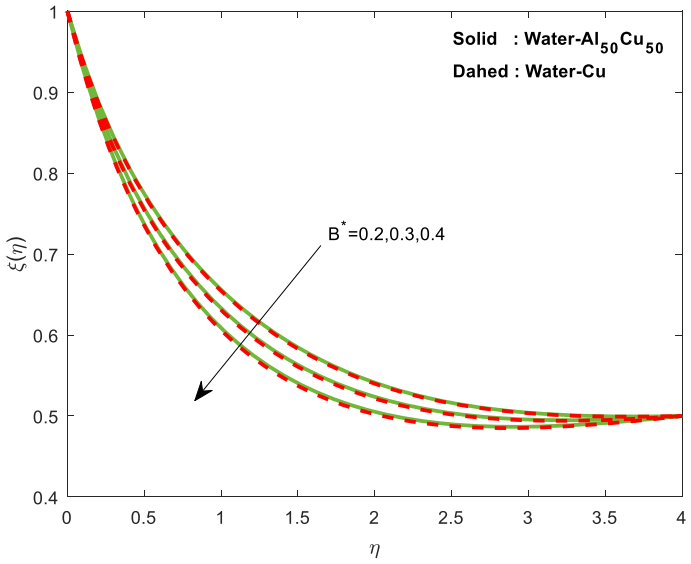

Fig. 16. Concentration behavior with variation in B^*.

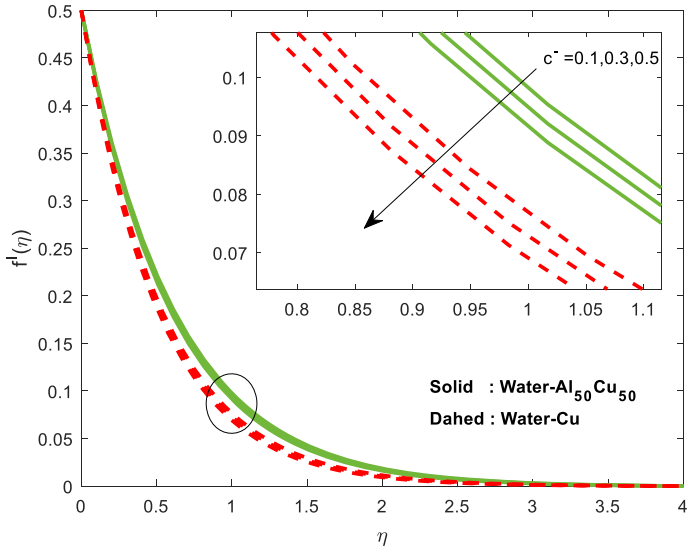

Fig. 17. Velocity behavior with variation in $\bar{c}$.

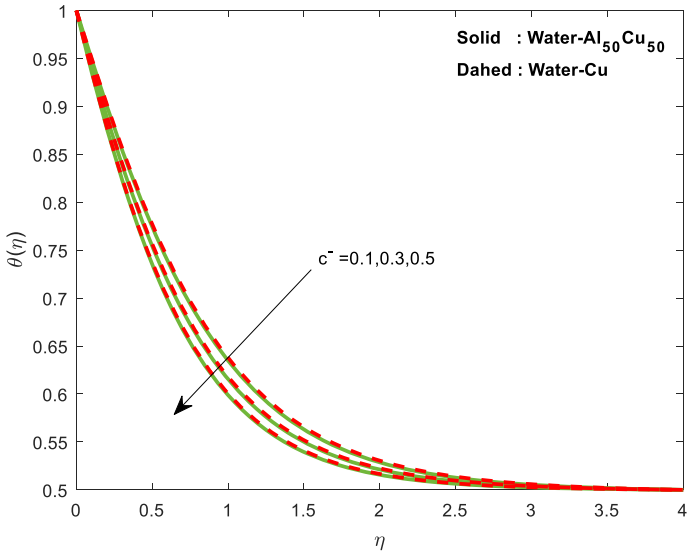

Fig. 18. Thermal behavior with variation in $\bar{c}$.

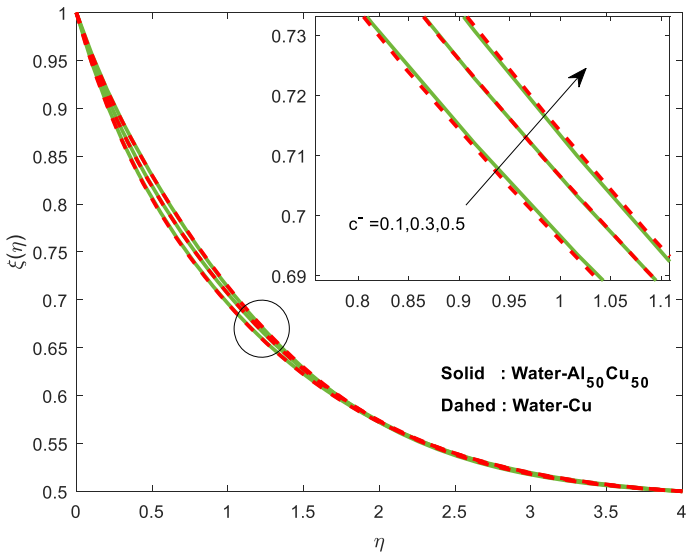

Fig. 19. Concentration behavior with variation in $\bar{c}$.

Table 1 shows the thermophysical properties of the nanomaterials and the base fluid. Tables 2, 3 give the response of Nu_x, Sh_x and C_f for various pertinent parameters for $Al_{50}Cu_{50}$-water and Cu-water nanofluids, respectively. It is found out that the friction factor of the Cu-water nanofluid drops rapidly as compared to the $Al_{50}Cu_{50}$-water nanofluid. A^* and B^* are recognized as the controlling parameters of the thermal transport rate, and ϕ can boost the local Nusselt number effectively in the $Al_{50}Cu_{50}$-water nanofluid compared with the Cu-water nanofluid. But, the converse behaviour is noticed for the local Sherwood number. Increasing values of Nt and Nb make the heat transport rate diminish and enhance the mass transport rate. The parameter Ec has a tendency to diminish the local Nusselt number and enhances the Sherwood number; on the other hand, exactly the contrary behaviour is found for the needle thickness parameter. Table 4 shows the validation of the computational results by comparing them with other techniques.

Table 1. Thermophysical properties of base fluid (water) and alloy nanoparticles at 300 K.

Physical properties	$Al_{50}Cu_{50}$	Cu	Water
C_p (J/Kg K)	747.90	385	4179
ρ (Kg/m^3)	4133.68	8933	997.3
K (W/m K)	112	400	0.613
σ (S/m)	1.4993×10^7	5.98×10^7	0.05

Table 2. Numerical values for C_f, Nu_x and Sh_x for the $Al_{50}Cu_{50}$-water nanofluid.

ϕ	M	Nt	Nb	Ec	A^*	B^*	$\bar{c}$	$f''(\bar{c})$	$-\theta'(\bar{c})$	$-\xi'(\bar{c})$
0.1								−1.263994	0.441984	0.548936
0.2								−1.764628	0.561734	0.561785
0.3								−2.515624	0.717394	0.570051
	1							−1.764628	0.561734	0.561785
	4							−2.666510	0.446067	0.656363
	8							−3.462796	0.350322	0.737761
		0.2						−1.764628	0.585991	0.553863
		0.5						−1.764628	0.561734	0.561785
		0.8						−1.764628	0.538111	0.594823
			0.4					−1.764628	0.570225	0.551974
			0.5					−1.764628	0.561734	0.561785
			0.6					−1.764628	0.553319	0.568268
				0.2				−1.764628	0.459219	0.653832
				0.3				−1.764628	0.356690	0.745891
				0.4				−1.764628	0.254147	0.837963
					1			−1.764628	0.478712	0.635944
					2			−1.764628	0.394832	0.710869
					3			−1.764628	0.310931	0.785813
						0.2		−1.764628	0.457069	0.655736
						0.3		−1.764628	0.397955	0.708772
						0.4		−1.764628	0.335768	0.764545
							0.1	−1.764628	0.561734	0.561785
							0.3	−3.122915	1.113209	0.511943
							0.5	−4.118401	1.621556	0.460650

Table 3. Numerical values for C_f, Nu_x and Sh_x for the Cu-water nanofluid.

ϕ	M	Nt	Nb	Ec	A^*	B^*	$\bar{c}$	$f''(\bar{c})$	$-\theta'(\bar{c})$	$-\xi'(\bar{c})$
0.1								−1.376563	0.433631	0.558033
0.2								−2.022478	0.549378	0.572419
0.3								−2.978360	0.705437	0.578649
	1							−2.022478	0.549378	0.572419
	4							−3.188180	0.425813	0.673290
	8							−4.202384	0.327092	0.757161
		0.2						−2.022478	0.573604	0.556265
		0.5						−2.022478	0.549378	0.572419
		0.8						−2.022478	0.525785	0.613561
			0.4					−2.022478	0.557828	0.566139
			0.5					−2.022478	0.549378	0.572419
			0.6					−2.022478	0.541004	0.576548
				0.2				−2.022478	0.437293	0.672704
				0.3				−2.022478	0.325193	0.773002
				0.4				−2.022478	0.213082	0.873311
					1			−2.022478	0.475514	0.638217
					2			−2.022478	0.400892	0.704691
					3			−2.022478	0.326257	0.771177
						0.2		−2.022478	0.442843	0.667870
						0.3		−2.022478	0.382581	0.721840
						0.4		−2.022478	0.319110	0.778667
							0.1	−2.022478	0.549378	0.572419
							0.3	−3.603919	1.093464	0.521871
							0.5	−4.784902	1.598291	0.469857

Table 4. Validation of the numerical technique for $-\xi'(\bar{c})$.

ϕ	ST	RKN	$bvp5c$	$bvp4c$
0.1	0.558033	0.5580334521	0.5580334520	0.5580334521
0.2	0.572419	0.5724197635	0.5724197634	0.5724197634
0.3	0.578649	0.5786493520	0.5786493520	0.5786493520
0.4	0.580902	0.5809027347	0.5809027346	0.5809027346

4 Conclusions

Aluminium and its alloys due to their substantial properties, such as the extreme corrosion resistance, extraordinary high electrical and thermal conductivities and ease of fabrication, achieved remarkable applications in transportation especially in space and aircraft and in the production of electrical transmission lines. In view of these, the current literature is integrated to probe the impact of thermophoretic and the Brownian moment on the boundary layer analysis of a 2D forced convection flow along a persistently moving horizontal needle with frictional heating effects. Magnetic nano-properties are incorporated in our study. The important outcomes of the present analysis are:

- Thermophoretic and Brownian moment parameters are capable to increase the thermal behavior of the fluid.
- The volume fraction parameter is more effective in enhancing the thermal conductivity.
- The needle thickness parameter enhances the energy transport rate, whereas it diminishes the mass transport rate.
- Larger values of A^* and B^* make the thermal boundary layer increase; whereas, they make the heat transfer rate decrease.
- The $Al_{50}Cu_{50}$-water nanofluid moves slightly faster as compared with the Cu-water nanofluid.

The authors acknowledge the UGC for financial support under the UGC Dr. D. S. Kothari Postdoctoral Fellowship Scheme (No. F.4-2/2006 (BSR)/MA/13-14/0026).

References

1. S.M.S. Murshed, K.C. Leong, C. Yang, Int. J. Therm. Sci. **44**, 367 (2005).
2. M. Hatami, R. Nouri, D.D. Ganji, J. Mol. Liq. **187**, 294 (2013).
3. M. Sheikholeslami, S. Abelman, D.D. Ganji, Int. J. Heat Mass Transfer **79**, 212 (2014).
4. A. Malvandi, M.R. Safaei, M.H. Kaffash, D.D. Ganji, J. Magn. & Magn. Mater. **382**, 296 (2015).
5. C. Sulochana, G.P. Ashwinkumar, N. Sandeep, J. Niger. Math. Soc. **35**, 128 (2016).
6. O.D. Makinde, F. Mabood, W.A. Khan, M.S. Tshehla, J. Mol. Liq. **219**, 624 (2016).
7. J. Buongiorno, J. Heat Transf. **128**, 240 (2006).
8. M. Jayachandra Babu, N. Sandeep, J. Mol. Liq. **222**, 1003 (2016).
9. C. Sulochana, G.P. Ashwinkumar, N. Sandeep, Alex. Eng. J. **55**, 1151 (2016).
10. M.A. Sheremet, D.S. Cimpean, I. Pop, Appl. Therm. Eng. **113**, 413 (2017).
11. G. Kumaran, N. Sandeep, J. Mol. Liq. **233**, 262 (2017).
12. L.L. Lee, Phys. Fluids **10**, 822 (1967).
13. C.Y. Wang, Phys. Fluids A Fluid Dyn. **2**, 622 (1990).
14. T. Grosan, I. Pop, ASME J. Heat Tranf. **133**, 054503 (2011).
15. R. Trimbitas, T. Grosan, Int. J. Numer. Methods Heat Fluid Flow **24**, 579 (2014).
16. T. Hayat, M.I. Khan, M. Farooq, T. Yasmeen, A. Alsaedi, J. Mol. Liq. **224**, 786 (2016).
17. S.K. Soid, A. Ishak, I. Pop, Appl. Therm. Eng. **114**, 58 (2017).
18. K.V. Prasad, K. Vajravelu, H. Vaidya, Int. J. Comput. Methods Eng. Sci. Mech. **17**, 288 (2016).
19. S.P.A. Devi, M. Prakash, J. Appl. Fluid Mech. Mech. **9**, 683 (2016).
20. M. Jayachandra Babu, N. Sandeep, Alex. Eng. J. **55**, 2193 (2016).
21. O.D. Makinde, I.L. Animasaun, J. Mol. Liq. **221**, 733 (2016).
22. J.V. Ramana Reddy, V. Sugunamma, N. Sandeep, J. Mol. Liq. **229**, 380 (2017).
23. R. Nazar, L. Tham, I. Pop, D.B. Ingham, Transp. Porous Media **86**, 517 (2011).
24. F.O. Pătrulescu, T. Groşan, I. Pop, Int. J. Numer. Methods Heat Fluid Flow **24**, 1175 (2014).
25. J.V.R. Reddy, V. Sugunamma, N. Sandeep, J. Mol. Liq. **223**, 1234 (2016).
26. C. Sulochana, G.P. Ashwinkumar, N. Sandeep, Int. J. Adv. Sci. Technol. **86**, 61 (2016).
27. A. Malvandi, S. Heysiattalab, D.D. Ganji, J. Mol. Liq. **216**, 503 (2016).
28. M. Jayachandra Babu, N. Sandeep, J. Mol. Liq. **232**, 27 (2017).
29. S. Corasaniti, F. Gori, Int. Commun. Heat Mass Transf. **81**, 72 (2017).
30. W.A. Khan, Z.H. Khan, R.U. Haq, Eur. Phys. J. Plus **130**, 86 (2015).
31. M. Sheikholeslami, D.D. Ganji, Alex. Eng. J. (2016) DOI: 10.1016/j.aej.2016.11.007.
32. J.V. Ramana Reddy, V. Sugunamma, N. Sandeep, J. Mol. Liq. **236**, 93 (2017).
33. N. Sandeep, Adv. Powder Technol. **28**, 865 (2017).